Met. Mater. Int., Vol. 22, No. 2 (2016), pp. 243~251
doi: 10.1007/s12540-016-5510-2

Pre-Aging Time Dependence of Microstructure and Mechanical Properties in Nanostructured Al-2wt%Cu Alloy

Bahram Azad[1,*] and Ehsan Borhani[2]

[1]Faculty of Metallurgical and Materials Engineering, Semnan University, Semnan, Iran
[2]Department of Nanotechnology, Nano-materials Group, Semnan University, Semnan, Iran

(received date: 15 September 2015 / accepted date: 19 November 2015)

This work is focused on the effect of pre-aging time on the properties of Al-2wt%Cu alloy processed by accumulative roll bonding (ARB) process. Following aged at 190 °C for 10 or 30 min, the samples were deformed up to a strain of 4.8 by the ARB process. The microstructure evolution was investigated by transmission electron microscope and electron backscattering diffraction analyzes. The results showed that the Al_2Cu precipitates were formed with different sizes due to the different pre-aging times and the finer precipitates were more effective on the formation of high angle grain boundaries during the ARB process. The grain size of Aged-10 min and Aged-30 min specimens decreased to 400 nm and 420 nm, respectively, after 6 cycles of the ARB process. Also, the final texture after 6 cycles of the ARB process, shown in the {111} pole figure, were different depending on the starting microstructures. The mechanical properties of specimens were investigated by the Vickers microhardness measurements and the tensile tests. The results showed that the mechanical properties are affected by the starting microstructure. The mechanical properties of Aged-10 min specimen were different compared to Aged-30 min specimen due to the different size of the pre-existing precipitates. Although by continuing process, the precipitates were probably dissolved due to the heavy deformation.

Keywords: aging, severe plastic deformation, nanostructured materials, microstructure, mechanical properties

1. INTRODUCTION

Interest in the processing of bulk ultrafine grained (UFG) materials through the application of severe plastic deformation (SPD) has significantly grown [1,2]. Several SPD techniques have been designed for achieving to high strength metals with minimal changes in initial sample dimensions. Some SPD techniques, such as equal channel angular pressing (ECAP) [3], high pressure torsion (HPT) [4], cyclic extrusion compression (CEC) [5] and accumulative roll bonding (ARB) [6] have been developed. Among these SPD techniques, ARB process allows to accumulate very large plastic strains into materials without changing the dimensions of material by repeating the process of cutting the rolled sheet, stacking them in the initial thickness and roll-bonding the stacked sheets again [6].

Deformation conditions such as strain, strain rate, temperature and strain path and also material parameters such as stacking fault energy, impurity level and presence of second phase particles control the formation of UFGs. For example, high strain rate deformation is one of the most influential factors on grain refinement during SPD processes or presence of second phase particle can be accelerated the formation of UFGs. Microstructure evolution, mechanical properties and texture evolution of ARB-processed alloys have been studied by many researchers [7-9], however, some characteristics of ARB-processed alloys such as effect of pre-aging process on microstructure evolution and mechanical properties of alloys during ARB process still need an in-depth research. One of the limited researches in this field was done by Borhani *et al*. [10,11]. Their results showed that the Aged-specimens have smaller grain size and higher mechanical properties than that of solution treated (ST) specimens. Also, Min *et al*. [12] reported that the alloy of aged and ARBed (Aged-ARB) has higher fraction of high-angle grain boundaries (HAGBs) than the alloy of solution treated and ARBed (ST-ARB) at the same strain level. Based on the previously studies, the presence of second phase particle could potentially have a significant effect on the properties of metals during ARB process. Tsuji *et al*. [13] reported that the temperature increases in the SPD process due to large plastic strain and it reaches to 130 °C at 1100 commercial purity aluminum during ARB process. However, Silcock *et al*. [14] showed that this increas-

*Corresponding author: Bahramazad1987@gmail.com

ing of temperature (130 °C) is not sufficient for precipitation in Al-2Cu alloy due to precipitation kinetics is very slow and almost no precipitation occurs at 130 °C for aging up to 10 days. Also, it is reported that only θ′ phase precipitates without GP zones at 190 °C in Al-2Cu alloy [14].

Precipitation strengthened Al alloys are good candidates for a production of thermally stable high-strength UFG materials. The binary Al-Cu system is a well-studied precipitation strengthening system because it forms the basis for a wide range of age-hardening alloys that are technologically important [15]. In the present study, the ARB process was carried out on Al-2wt%Cu alloy with different starting microstructures in order to research on the effect of pre-aging time on the microstructure evolution and the mechanical properties during the ARB process.

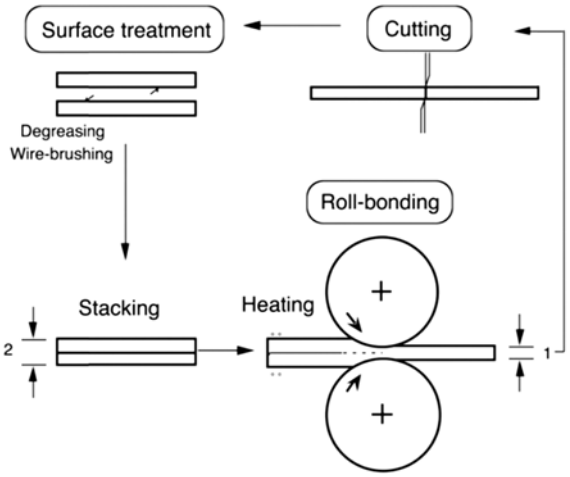

Fig. 1. Schematic illustration of ARB process [6].

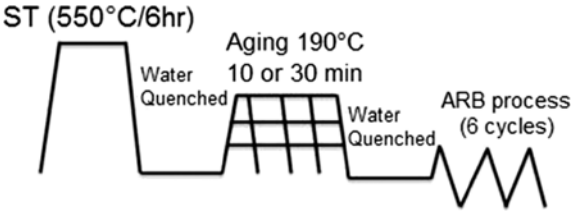

Fig. 2. Schematic illustration of the thermal and the mechanical processes used in this study.

2. EXPERIMENTAL PROCEDURES

An Al-2wt%Cu alloy was prepared as sheets with a thickness of 2 mm, a width of 60 mm and a length of 200 mm. The chemical composition of alloy used in the present study is given in Table 1.

The sheets were solution-treated at 550 °C/6hr and immediately quenched in the water. Some of the ST sheets were aged at 190 °C for 10 or 30 min, to obtain very fine Al_2Cu precipitates with different sizes. These two types of the sheets were used as the starting materials for the ARB process. The starting sheets with a thickness of 2 mm were firstly cold-rolled by 50% reduction in the thickness that named as the first ARB cycle. The 50% rolled sheets of 1 mm thick were cut into two pieces. To prepare of the sheets and create a satisfactory bond in the ARB process, the surfaces of sheets were cleaned by acetone and roughened by a wire brush and then roll-bonded by 50% reduction in one pass at room temperature as shown in Fig. 1. The same procedures were repeated up to 6 cycles including the first cold-rolling, which corresponded total equivalent strain of 4.8. The ARB process was immediately carried out to avoid for any oxide formation. The ARB process was carried out by two mills with 110 mm diameter rolls with rolling speed of 29 rpm. The thermal and the mechanical procedures used in this study are schematically shown in Fig. 2. Sections normal to the transverse direction (TD) of the sheets were used for the microstructural observations. Electron backscattering diffraction (EBSD) analysis was carried out in a scanning electron microscope (SEM) with a field emission type gun (FE-SEM; Philips XL30) operated at 15 kV using a step size of 0.05 μm. The specimens were mechanically polished and then electro-polished in a solution of 30% HNO_3 and 70% CH_3OH before the measurements. The transmission electron microscope (TEM) observations were carried out using Hitachi H-800 operated at 200 kV. Thin foil specimens normal to TD were prepared through mechanical polishing firstly down to approximately 70 μm in the thickness, and then electropolishing in the same solution as that for the EBSD specimens. The misorientation was calculated between neighboring measured points in the EBSD mapping data by software (OIM analysis software version 5.6). Pole figures are used for the texture analysis in this study. The orientations are represented by the expression of {h k l} <u v w>, where {h k l} represents the Miller index of the crystallographic plane parallel to the rolling plane and <u v w> represents the Miller index of the crystallographic direction parallel to the rolling direction (RD). The mechanical properties of the specimens were investigated by the Vickers microhardness measurements and the tensile tests. The tensile tests were carried out using Gotech 100 KN tensile machine at the initial strain rate 8×10^{-3} s^{-1} at room temperature. The tensile test specimens were machined from the rolled sheets according to the ASTM-E 8M standard, oriented along the RD. On the other

Table 1. The chemical composition of Al-2wt%Cu alloy

Alloying elements	Cu	Mg	Fe	Si	Mn	Cr	Ti	Al
wt%	1.96	0.001	0.022	0.004	0.001	0.006	0.0001	base

hand, the mean value of hardness was evaluated by Buehler MMT-7 microhardness tester using a load of 0.05 Kgf and a loading period of 10 s at room temperature.

3. RESULTS AND DISCUSSION

The TEM micrographs of specimens before the ARB process are shown in Fig. 3. As shown in this figure, Ashby-Brown contrasts [16,17] are used to understand the degree of coherency between a particle and the matrix. The Ashby and Brown contrast consists of spherical strain lines and irregular strain lines. The Ashby and Brown contrast appears around a spherical coherent precipitate in bright-field images. Loss of spherical strain caused by the introduction of interfacial dislocations is detected by the irregularity of the strain lines in the Ashby-Brown contrast. It is well known that the spherical strain lines appear around a spherical coherent particle, whereas irregular strain lines appear inside a semi-coherent. As shown in this figure, there are very fine Al_2Cu precipitates with different sizes. The average size of Al_2Cu precipitates are 10 nm and 16 nm for the Aged-10 min and the Aged-30 min specimens, respectively. The aging behavior of alloys depends on aging temperature and aging time. Here, it is noteworthy that the aging time affects the size of precipitates and with increasing the aging time, the average size of precipitates

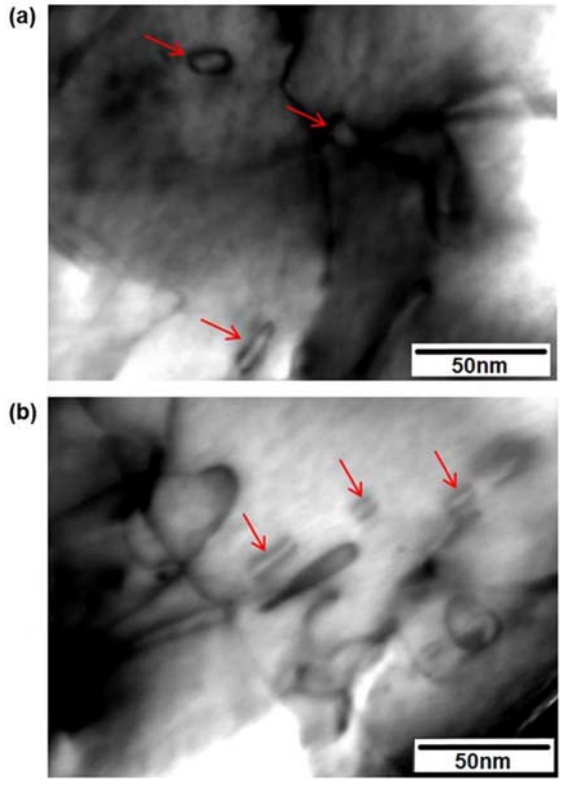

Fig. 3. TEM micrographs of (a) Aged-10 min and (b) Aged-30 min specimens before the ARB cycles showing the fine precipitates (indicated by arrows).

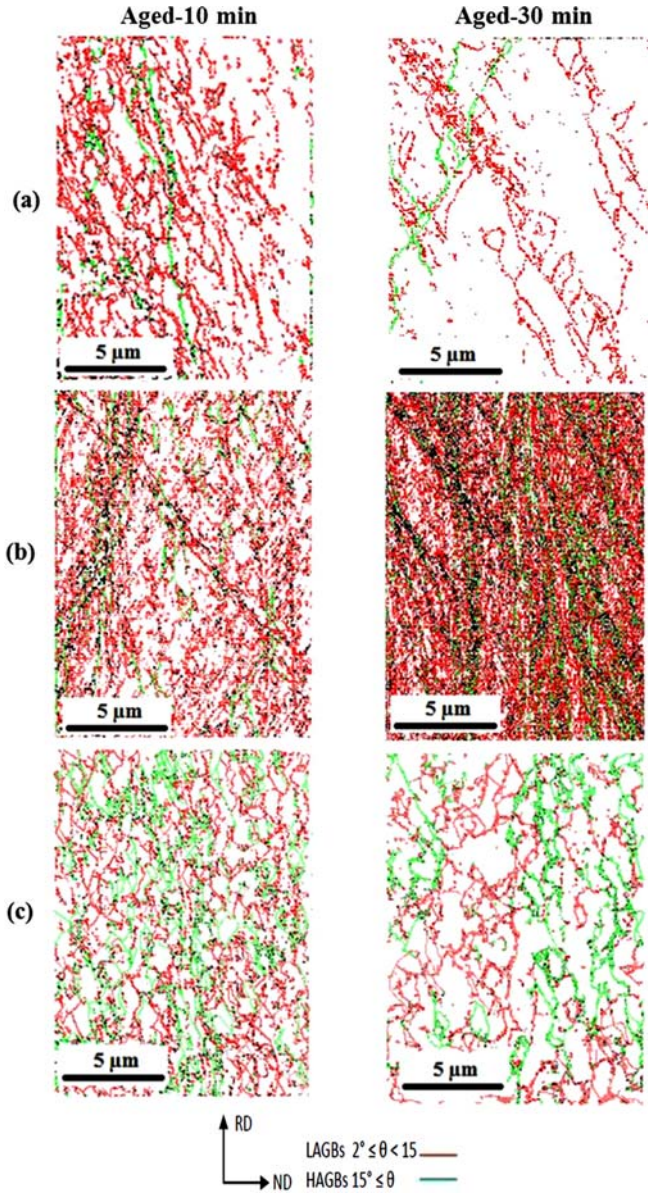

Fig. 4. Grain boundary maps obtained from the EBSD measurement for the Aged-ARB specimens at (a) 1, (b) 3, and (c) 6 cycles.

increases. However, there is not much difference between the average size of precipitates due to the small difference between times of pre-aging process used in this study.

Grain boundary maps obtained from the EBSD analysis of the aged specimens after various cycles of the ARB process are shown in Fig. 4. In the boundary map, HAGBs with misorientation angles above 15° are shown as green lines, while low-angle grain boundaries (LAGBs) with misorientation angles between 2° and 15° are shown as red lines. Boundaries with misorientation smaller than 2° were removed in order to raise the reliability. The fraction of HAGBs (f_{HAGBs}) obtained from the EBSD measurements of the ARBed specimens are given in Fig. 5. The f_{HAGBs} increases with increas-

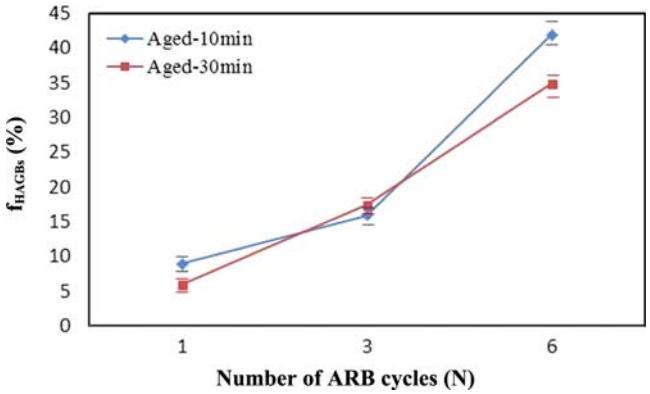

Fig. 5. The fraction of HAGBs as a function of the number of ARB cycles.

ing the number of the ARB cycles. As can be seen, there are a few elongated subgrains and a lot of equiaxed grains and subgrains with a high fraction of LAGBs after the initial cycle in both specimens. One of the reasons for the formation of equiaxed grains in FCC metals can be continuous recrystallization that existence of recrystallized grains due to large strain at room temperature have been reported by some researchers [18,19]. After 1-cycle ARB process, the f_{HAGBs} of Aged-10 min and Aged-30 min specimens are 8% and 6%, respectively. On the other hand, after 6 cycles of ARB process, the f_{HAGBs} increases to 42% and 35% for the Aged-10 min and the Aged-30 min specimens, respectively. The results show that the rate of HAGBs formation is affected by the time of pre-aging process and the finer precipitates are more effective for the formation of HAGBs. These results are consistent with the previous studies on ARB process [10-12].

The misorientation distributions obtained from the EBSD measurements of ARBed specimens are given in Fig. 6 as fraction-misorientation histograms. As can be seen in this

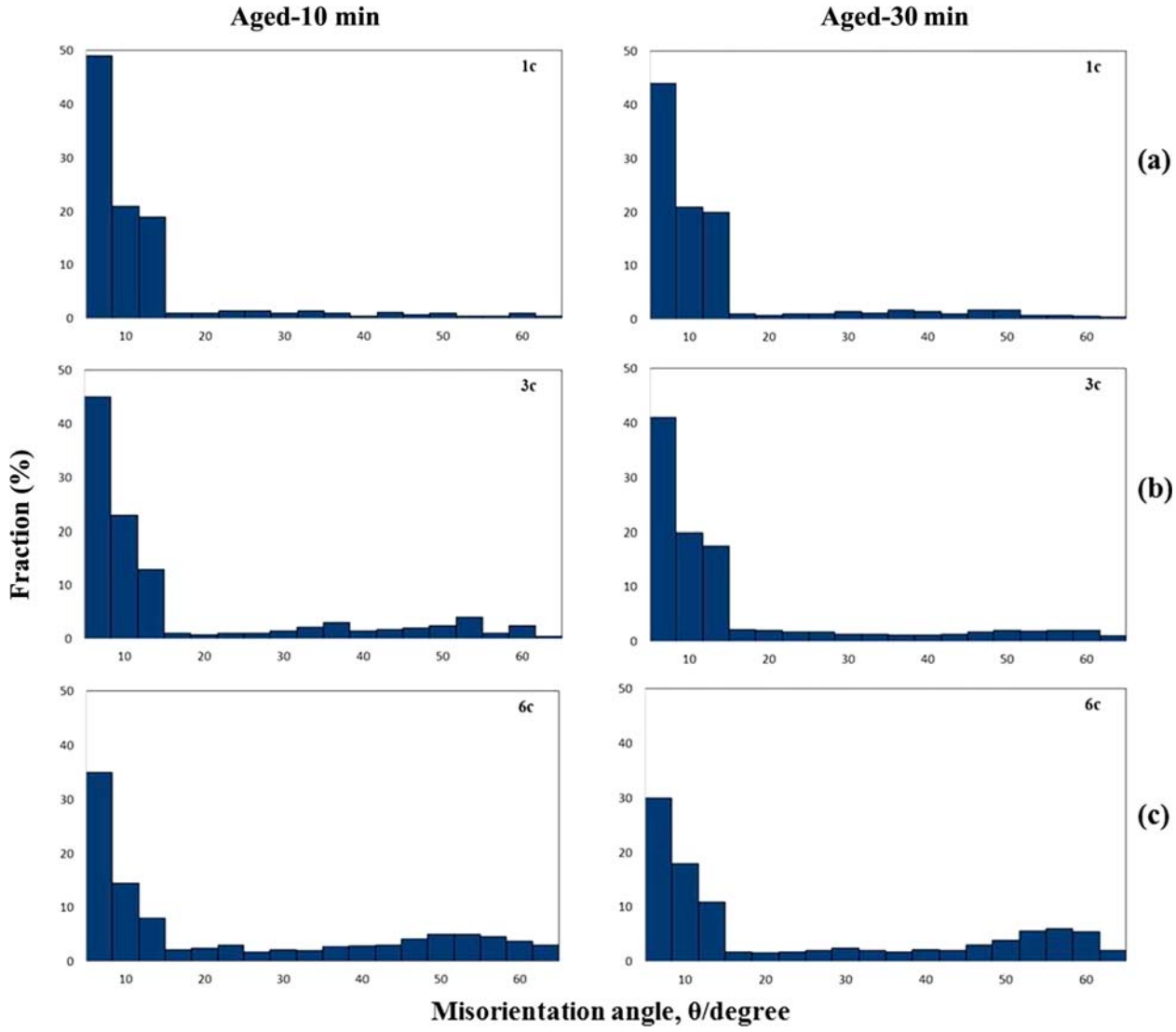

Fig. 6. Misorientation distribution in the Aged-specimens after (a) 1, (b) 3, and (c) 6 cycles of the ARB process.

figure, after 1-cycle ARB process, the shape of histogram is similar and the fraction of boundaries with misorientation less than 5° is very high. By continuing the ARB process, the fraction of LAGBs (f_{LAGBs}) decreases while the f_{HAGBs} increases. After 3-cycle ARB process, the f_{LAGBs} decreases in the all of specimens, while the f_{HAGBs} is not still high. With increasing the number of the ARB cycles up to 6-cycle ARB process, the f_{HAGBs} drastically increases in the specimens. After 6-cycle ARB process, the f_{HAGBs} ranging from 45° to 60° is the highest in the Aged-10 min specimen, while the

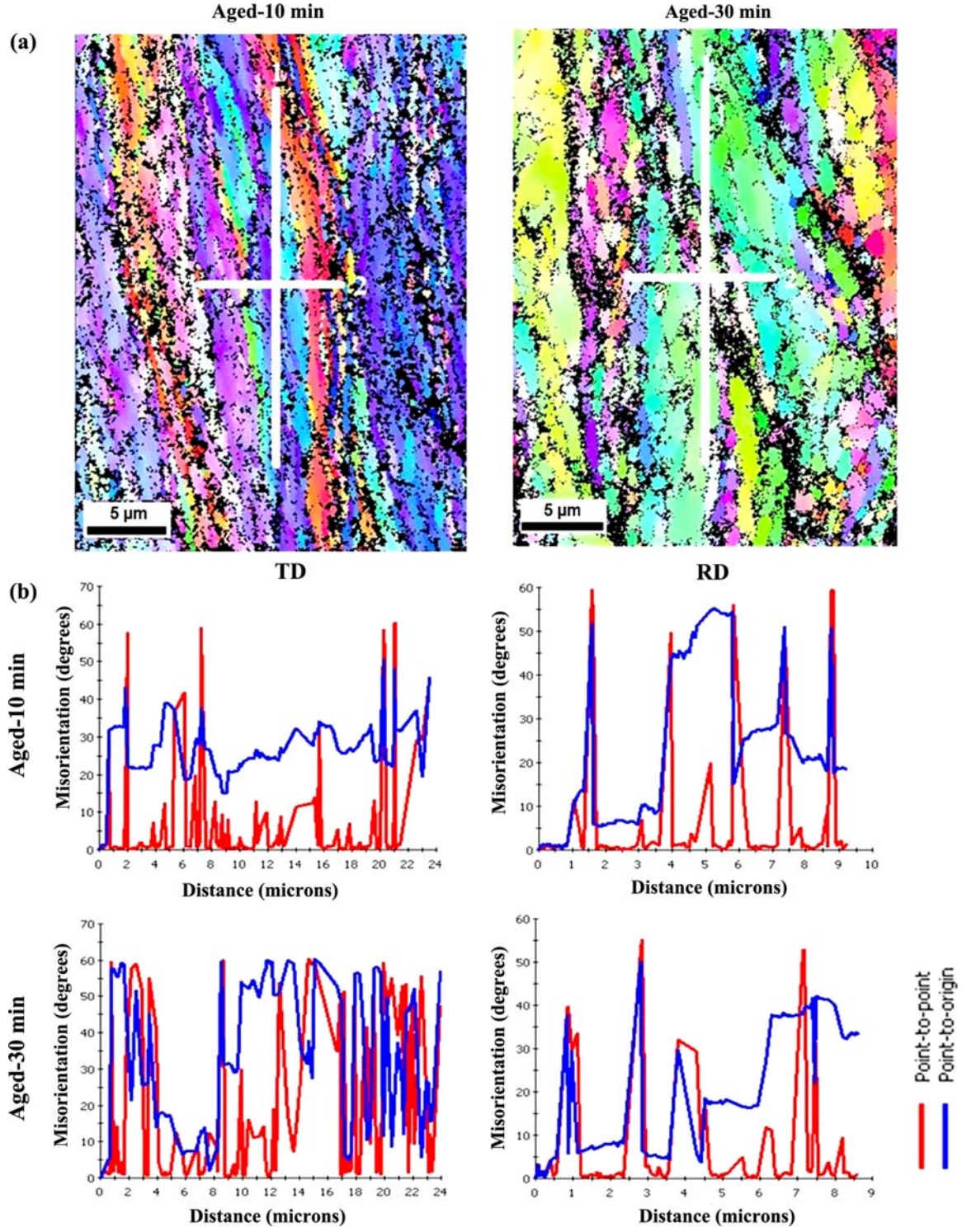

Fig. 7. (a) EBSD micrograph of the Aged specimens, (b) Misorientation profile along transvers boundaries (TD) (line 1 in (a)) and lamellar boundaries (RD) (line 2 in (a)) for the Aged-specimens after 6 cycles of ARB process.

f_{HAGBs} ranging from 55° to 60° is the highest in the Aged-30 min specimen. The results show that the aging time affects the misorientation distribution due to the difference in the starting microstructures. Also, the misorientation is changed from low angle to high angle at each cycle due to the strain evolution. These results indicate that the maximum rate of grain refinement is related to the first cycle and then decreases at higher cycles. This observation can be explained by saturation phenomenon where the formation of new dislocation in the deformed grains is difficult [20, 21].

There exist two types of boundaries in the ARB processed specimens; the lamellar boundaries parallel to the rolling direction and the transverse boundaries interconnecting the lamellar boundaries. Figure 7 shows the misorientation profiles along two transverse and lamellar boundaries of the 6th ARB processed specimen which are indicated with line 1 and line 2, respectively. The misorientation profiles show higher misorientation for transverse boundaries compared to those lamellar boundaries [22].

The changes in the grain size are given in Fig. 8. The grain size is evaluated as the mean spacing of HAGBs along normal direction (ND) by linear intercept method in the EBSD boundary maps. As shown in this figure, the mean grain size of specimens decreases with increasing the number of the ARB cycles and decreases to 400 nm and 420 nm for the Aged-10 min and the Aged-30 min specimens after 6-cycle ARB process, respectively. As can be seen, the mean grain size of the Aged-10 min specimen is smaller than that of the Aged-30 min specimen in the initial cycles. It should be noted that after 3-cycle ARB process the mean grain size of specimens is not much different to each other. The results show that the specimen containing smaller precipitates has a rapid rate of grain refinement in the initial cycles. On the other hand, with increasing the number of the ARB cycles, the rate of grain refinement decreases in the Aged-10 min specimen, so that the grain size of specimens has almost no much difference after 6-cycle ARB process. It is well known that fine precipitate can inhibit grain boundary migration by

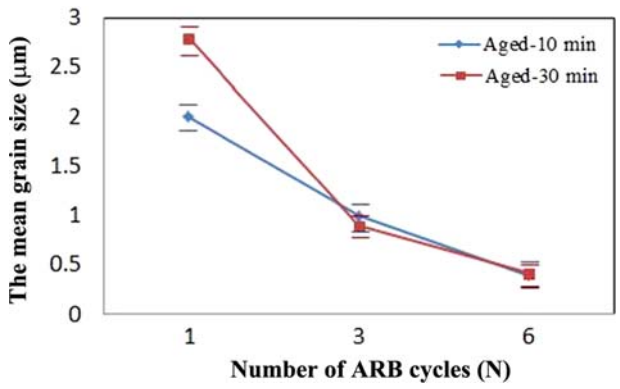

Fig. 8. The mean grain size of the specimens as a function of the number of ARB cycles.

so-called Zener drag effect. The fine precipitates with narrow interparticle spacing can also transmit higher Zener force F to the boundaries. The Zener dragging force, F, is shown as follows [23,24]:

$$F = \frac{3}{8}\left(\frac{f}{r^2}\right)\gamma D_g \quad \text{for a low grain boundary} \tag{1}$$

$$F = \frac{3}{2}\left(\frac{f}{r^2}\right)\gamma D_g \quad \text{for a high grain boundary} \tag{2}$$

where f is the volume fraction of second phase particles, r is the mean particle radius, Dg is the size of the grains and γ is the interface energy. It is found that F becomes larger when the Al_2Cu precipitates have finer size (r) and keep identical orientation to the matrix, which results in lower interface energy (γ) [23,24]. Therefore, the Al_2Cu precipitates must have fine particle size, narrow interparticle spacing and coherency with matrix in order to effectively transmit Zener force to the alloy. Based on the experimental results, the Aged-10 min specimen with the finer pre-existing precipitates shows the smaller grain size than the Aged-30 min specimen. The results also qualitatively agree with the magnitude of Zener dragging force expected from the Eqs. (1) and (2).

The {111} pole figures of the specimens after various cycles of the ARB process are shown in Fig. 9. As shown in Fig. 9, Copper {112} <111> component is a main texture by 1-cycle ARB process in both specimens. G {110} <001> component is developed as a main texture by 3-cycle ARB process in the Aged-10 min specimen. The texture is changed to Copper {112} <111> component with increasing the number of the ARB cycles up to 6 cycles of the ARB process. Copper {112} <111> component is developed as a main texture by 3-cycle ARB process in the Aged-30 min specimen and changed to S {123} <634> component after 6 cycles of the ARB process. It can be concluded that the texture transition occurs during the ARB process in all of the specimens, however, the final texture after 6 cycles and the distribution in the {111} pole figure are different depending on the starting microstructures. The difference between the microstructure evolutions of the specimens could be attributed to the difference between the size of precipitates due to the different aging times.

Figure 10 shows the Vickers microhardness value of Aged-10 min and Aged-30 min specimens during the ARB process. The microhardness value is affected by both the grain refinement and the pre-existing precipitates [10,11]. The Vickers microhardness values of Aged-10 min and Aged-30 min specimens are 86 HV and 79 HV before the ARB process (0-cycle ARB), respectively. The hardness value of the specimens considerably increases after 1-cycle ARB process. On the other hand, the hardness value of the specimens is enhanced with increasing the number of the ARB cycles. This increasing continues up to 4-cycle ARB process for the Aged-10 min

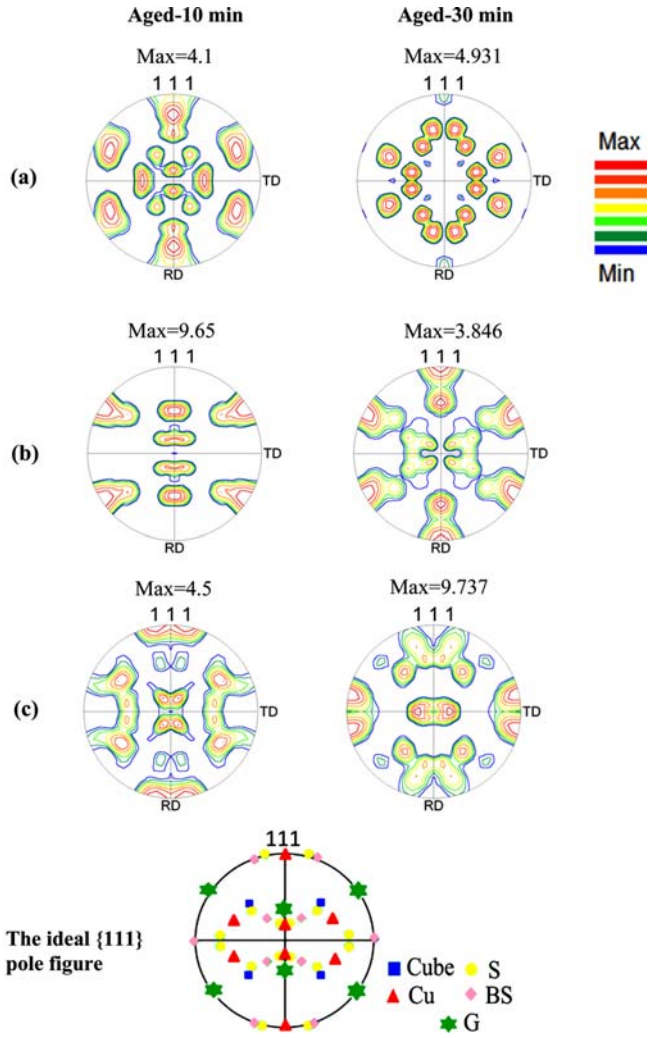

Fig. 9. {111} pole figures of the Aged-ARB specimens after (a) 1, (b) 3, and (c) 6 cycles of the ARB process (containing the ideal {111} pole figure).

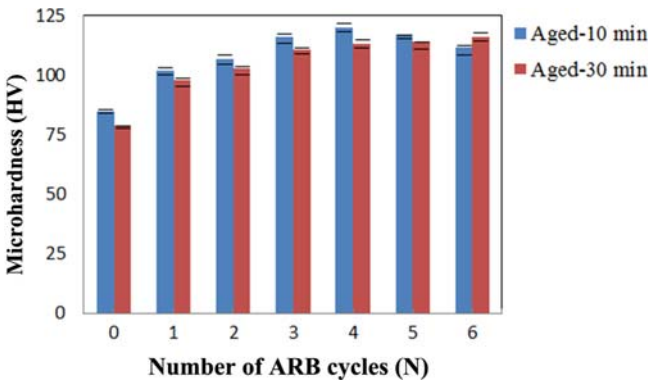

Fig. 10. The Vickers microhardness of the specimens processed by various cycles of the ARB process.

specimen and the hardness value decreases with further ARB cycles but at a progressively low rate. The difference between the hardness values of specimens is probably due to the size of Al_2Cu precipitates which precipitates inhibit dislocation motion and harden the materials [10]. Also, the increase in the hardness value can be due to the grain refinement and the reduction in the grain size increases the hardness value. It should be noted that the results show the pre-existing precipitates have a more effect on the increase of microhardness value in the initial cycles. As can be seen, the hardness value does not have a significant difference between the specimens after 6-cycle ARB process. This indicates that with further ARB cycles, the effect of precipitates decreases due to the large plastic strains. Large plastic strains induced by SPD process can dissolve or fragment the precipitates [10-12,25]. The efficiency of precipitates depends on their size, internal properties, and distribution through the lattice [26-27]. Therefore, one of the reasons for the reduction of hardness in the Aged-10 min specimen after the final cycles of ARB process compared to the Aged-30 min specimen can be probably due to the difference between the size and the distribution of precipitates [11], which can be seen in Fig. 3, because of the different times of pre-aging process. As it has been reported before [10-12,26], it can be said that the large plastic strains have the different effects on the precipitates during the ARB process, depending on size and distribution of second phases within the matrix. As the process progresses, the difference between the hardness value of specimens decreases and there is no significant difference between the hardness of specimens after 6-cycle ARB process. As mentioned earlier, the hardness value of Aged-10 min specimen decreases after the final cycles. On the other hand, Aged-30 min specimen shows a saturation value of the hardness.

The variation of yield strength, tensile strength and uniform elongation of the specimens are shown in Fig. 11. The yield strength of Aged-10 min and Aged-30 min specimens are 90 MPa and 73 MPa before the ARB process, respectively. On the other hand, the tensile strength of Aged-10 min and Aged-30 min specimens are 137 MPa and 122 MPa before the ARB process, respectively. The points of yield strength and tensile strength are drastically increased by 1-cycle ARB process. As can be seen in Fig. 11, the yield strength and the tensile strength of Aged-30 min specimen increase with increasing the number of the ARB cycles, although with the slower rate between 1-cycle ARB to 6-cycle ARB, while these increments continue up to 3-cycle ARB in the Aged-10 min specimen and they are decreased with further ARB cycles up to 6-cycle ARB process. These results correspond well with the change in the hardness during the ARB process. Also as can be seen in this figure, the uniform elongation of the specimens is drastically decreased by 1-cycle ARB process. The uniform elongation of Aged-10 min specimen is 24% before the ARB process and decreases to 5.8% after 1-cycle ARB process. On the other hand, the uniform elongation of Aged-30 min specimen is 27% before the ARB process and

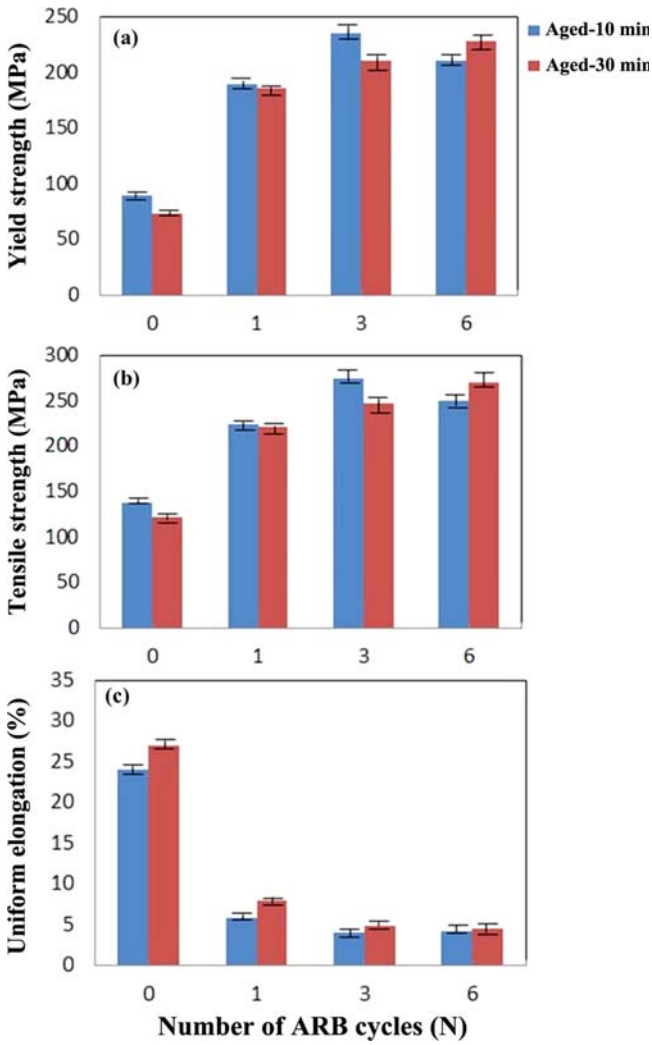

Fig. 11. The results of (a) yield strength, (b) tensile strength, and (c) uniform elongation after various cycles of the ARB process.

it decreases to 7.9% after 1-cycle ARB process. By continuing the process, the values of the uniform elongations are nearly shown a constant value about 4.5% in the both specimens. It can be concluded that the difference between the starting microstructures affects the mechanical properties of the specimens. This issue is clearly seen in Fig. 11 and also it has been previously shown in the Vickers microhardenss measurements. The results also show that the ARB process increases the yield strength and the tensile strength while the elongation decreases. Similar trends have been observed in the processed aluminum alloys [7,8,11]. The ARB processed specimens have dislocation substructure and elongated grain inside the UFG structures. These structures indicate that the strength of ARB processed specimens can be affected by grain refinement strengthening and also strain hardening. It has been reported that the increase of strength resulted from work hardening is dominant at the initial cycles to the medium cycles of ARB process [28]. It should be noted that the pre-existence precipitates have a strong effect on the mechanical properties of the alloy due to the precipitate hardening. It should be mentioned that the results show that the pre-existing precipitates have a significant effect on mechanical properties at relatively low strains. Therefore, it can be concluded that the precipitates may be fragmented or dissolved due to the large plastic strains with further SPD cycles [10-12,25]. Also, the pre-aging time of 10 min has a more effect on the mechanical properties before ARB process and during the initial cycles. As ARB progresses, the mechanical properties of Aged-10 min specimen slightly drop. This issue can be related to the dissolution of precipitates during the final cycles. Also, it has been reported that dissolving of the precipitates occurs during the ARB process which affects the mechanical properties of the deformed specimens [10].

4. CONCLUSION

The pre-aged Al-2wt%Cu sheets were processed by the ARB process up to a strain of 4.8. The effect of different pre-aging times on the microstructure evolution and the mechanical properties of the Al-2wt%Cu alloy during the ARB process were investigated in detail. The results are summarized as follows:

(1) The TEM micrographs of the specimens before the ARB process showed the precipitates of Al_2Cu with mean particle size of 10 nm and 16 nm for the Aged-10 min and the Aged-30 min specimens, respectively.

(2) The f_{HAGBs} increased with increasing the number of the ARB cycles. After 6-cycle ARB process, the f_{HAGBs} reached to 42% and 35% for the Aged-10 min and the Aged-30 min specimens, respectively. On the other hand, the rate of HAGBs formation was affected by the time of pre-aging process, and that the finer precipitates were more effective for the formation of HAGBs.

(3) The pre-aging time affected the misorientation distribution due to the different starting microstructures. After 6-cycle ARB process, the f_{HAGBs} ranging from 45° to 60° was the highest in the Aged-10 min specimen, while the f_{HAGBs} ranging from 55° to 60° was the highest in the Aged-30 min specimen.

(4) The mean grain size of the specimens decreased with increasing the number of the ARB cycles and decreased to 400 nm and 420 nm for the Aged-10 min and the Aged-30 min specimens after 6-cycle ARB process, respectively. The specimen containing smaller precipitates had a rapid rate of the grain refinement in the initial cycles. On the other hand, with increasing the number of the ARB cycles, the rate of grain refinement decreased in the Aged-10 min specimens, such that the grain size of the specimens was almost same after 6-cycle ARB process.

(5) Copper {112} <111> component was a main texture by 1-cycle ARB process in the both Aged-10 min and Aged-

30 min specimens. G {110} <001> component was developed as a main texture by 3-cycle ARB process in the Aged-10 min specimen and changed to Copper {112} <111> component with increasing the number of the ARB cycles up to 6 cycles. On the other hand, Copper {112} <111> component was developed as a main texture by 3-cycle ARB process in the Aged-30 min specimen and changed to S {123} <634> component after 6-cycle ARB process. The final texture after 6 cycles of ARB process and the distribution in the {111} pole figure were different depending on the starting microstructures.

(6) The Vickers microhardness values of Aged-10 min and Aged-30 min specimens before the ARB process were 86 HV and 79 HV, respectively. The difference between the hardness of specimens was probably due to the size of Al_2Cu precipitates which inhibit dislocation motion and harden the materials. By continuing process, there was no significant difference between the hardness values of the specimens.

(7) The pre-existing precipitates had a significant effect on the mechanical properties at relatively low strains. Also, the pre-aging time of 10 min had a more effect on the improvement of mechanical properties before the ARB process and also in the initial cycles. By continuing process, the mechanical properties of Aged-10 min specimen slightly dropped. This issue could be related to the dissolution of precipitates at the final cycles.

REFERENCES

1. B. Azad and E. Borhani, *J. Min. Metall. Sect. B* (In press).
2. E. Borhani, H. Jafarian, H. Adachi, D. Terada, and N. Tsuji, *J. Mater. Sci. Forum* **667-669**, 211 (2010).
3. R. Z. Valiev and T. G. Langdon, *Prog. Mater.* **51**, 881, (2006).
4. R. Z. Valiev, R. K. Islamgaliev, and I. V. Alexandrov, *Prog. Mater. Sci.* **45**, 103 (2000).
5. M. Richert, Q. Liu, and N. Hansen, *Mater. Sci. Eng. A* **260**, 27 (1999).
6. Y. Saito, H. Utsunomiya, N. Tsuji, and T. Sakai, *Acta Mater.* **47**, 579 (1999).
7. E. Borhani, H. Jafarain, A. Shibata, and N. Tsuji, *J. Mater. Trans.* **53**, 1863 (2012).
8. S. H. Lee, Y. Saito, T. Sakai, and H. Utsunomiya, *Mater. Sci. Eng. A* **325**, 228 (2002).
9. V. D. Cojocaru, D. Raducanu, D. M. Gordin, and I. Cinca, *J. Alloy Compd.* **546**, 260 (2013).
10. E. Borhani, H. Jafarian, D. Terada, H. Adachi, and N. Tsuji, *Mater. Trans.* **53**, 72 (2011).
11. E. Borhani, H. Jafarian, T. Sato, D. Terada, Y. Miyajima, and N. Tsuji, *Proc. 12th Intern. Conf. on Al. Alloy*, p.2168, Japan (2010).
12. B. K. Min, H. W. Kim, and S. B. Kang, *J. Mater. Proc. Tech.* **162-163**, 355 (2005).
13. N. Tsuji, T. Toyoda, Y. Minamino, Y. Koizumi, T. Yamane, M. Komatsu, and M. Kiritani, *Mater. Sci. Eng. A* **350**, 108 (2003).
14. J. M. Silcock, T. J. Heal, and H. K. Hardy, *J. Inst. Met.* **82**, 239 (1953-1954).
15. A. Biswas, D. J. Siegel, C. Wolverton, and D. N. Seidman, *Acta Mater.* **59**, 6187 (2011).
16. X. Huang, N. Tsuji, N. Hansen, and Y. Minamino, *Mater. Sci. Eng. A* **340**, 265 (2003).
17. B. G. Clark, I.M. Robertson, and L. M. Dougherty, *Mater. Res*. **20**, 1792 (2005).
18. F. Salimyanfard, M. Reza Toroghinejad, F. Ashrafizadeh, and M. Jafari, *Mater. Sci. Eng. A* **528**, 5348 (2011).
19. C. Xu, M. Furukawa, Z. Horita, and T. G. Langdon, *Acta Mater.* **51**, 6139 (2003).
20. Y. Iwahashi, Z. Horita, M. Nemoto, and T. G. Langdon, *Acta Mater.* **46**, 3317 (1998).
21. K.-T. Park, H.-J. Kwon, W.-J. Kim, and Y.-S. Kim, *Mater. Sci. Eng. A* **316**, 145 (2001).
22. X. Huang, N. Tsuji, N. Hansen, and Y. Minamino, *Mater. Sci. Eng. A* **340**, 265 (2003).
23. L. S. Toropova, D. G. Eskin, M. L. Kharakterova, and T. V. Dobatkina, *Advanced Aluminum Alloys Containing Scandium: Structure and Properties*, Gordon and Breach Science, The Netherlands (1998).
24. F. J. Humphreys and M. Hatherly, *Recrystallization and Related Annealing Phenomena*, pp.73-87, Pergamon Press, Oxford (1995).
25. Z. Horita, K. Oh-ishi, and K. Kaneko, *Sci. Tech. Adv. Mater.* **7**, 649 (2006).
26. G. F. Carter and D. E. Paul, *Materials Science and Engineering*, p.81, Materials Park, ASM International, Ohio (1991).
27. B. Azad and E. Borhani, *J. Mat. Eng. Per.* **24**, 4789 (2015).
28. K. T. Park, H. J. Kwon, W. J. Kim, and Y. S. Kim, *Mater. Sci. Eng. A* **316**, 145 (2001).